Nonlinear optical molecular switches for alkali ion identification

Plaquet, Aurélie; Champagne, BenoÎt; Castet, Frédéric

Published in:
Molecules

DOI:
10.3390/molecules190710574

Publication date:
2014

Document Version
Publisher's PDF, also known as Version of record

Molecules **2014**, *19*, 10574-10586; doi:10.3390/molecules190710574

OPEN ACCESS

molecules

ISSN 1420-3049

www.mdpi.com/journal/molecules

Article

Nonlinear Optical Molecular Switches for Alkali Ion Identification

Aurélie Plaquet [1,*], Benoît Champagne [1] and Frédéric Castet [2]

[1] Laboratoire de Chimie Théorique, UCPTS, Université de Namur (UNamur), rue de Bruxelles 61, B-5000 Namur, Belgium; E-Mail: benoit.champagne@unamur.be

[2] Institut des Sciences Moléculaires (ISM), Université de Bordeaux, UMR 5255 CNRS, Cours de la Libération 351, F-33405 Talence Cedex, France; E-Mail: f.castet@ism.u-bordeaux1.fr

* Author to whom correspondence should be addressed; E-Mail: aurelie.plaquet@unamur.be; Tel.: +32-0-81-724-554.

Received: 6 May 2014; in revised form: 23 June 2014 / Accepted: 7 July 2014 / Published: 21 July 2014

Abstract: This work demonstrates by means of DFT and *ab initio* calculations that recognition of alkali cations can be achieved by probing the variations of the second-order nonlinear optical properties along the commutation process in spiropyran/merocyanine systems. Due to the ability of the merocyanine isomer to complex metal cations, the switching between the two forms is accompanied by large contrasts in the quadratic hyperpolarizability that strongly depend on the size of the cation in presence. Exploiting the nonlinear optical responses of molecular switches should therefore provide powerful analytical tools for detecting and identifying metal cations in solution.

Keywords: nonlinear optics; molecular switches; alkali ion sensing; hyper-Rayleigh scattering; quantum chemical calculations; merocyanine/spiropyran

1. Introduction

For a few years now, the design of molecular switches with large nonlinear optical (NLO) contrasts has been the focus of a lot of experimental and theoretical investigations [1–4]. These systems, characterized by their ability to alternate between two or more different chemical forms displaying contrasts in one of their NLO properties, are of particular interest in the development of new photonic technologies including frequency doublers, space communications or biomedical imaging [5,6]. The commutation can be triggered by using various external stimuli such as a variation of pH [7–9],

temperature [10], light [11–13], redox potential [14–16], or solvent polarity. At the molecular scale, the property to optimize is usually the first hyperpolarizability (β), which is defined as the second-order response of the electric dipole moment (μ) to an external electric field, whereas a few studies have reported molecules with second hyperpolarizability (γ) contrasts [17]. A wide variety of NLO switches have been proposed, based e.g., on the indolino-oxazolidine [7–9,18,19], anil [11,20–23] or spiropyran [24] moieties, in which the amplitude of the β contrasts can be modulated by structural modifications and chemical functionalizations, *i.e.*, by varying the nature and length of the π-conjugated backbone, and/or the nature and position of donor and acceptor substituents.

Recently, we demonstrated by means of *ab initio* calculations that NLO switches based on the merocyanine/spiropyran equilibrium could also be exploited for selective identification of metal ions, thanks to the ability of the merocyanine form to complex cationic species such as alkali, alkaline earth, or transition metal ions. The design of molecular sensors able to recognize cations is of technological relevance with respect to many ecological, toxicological, or chemical issues [25,26]. In merocyanine/spiropyran systems, the commutation processes were shown to induce large NLO contrasts that depend on the nature of the cation involved, providing therefore a powerful detection tool [27] complementary to standard techniques based on variations in the absorption or fluorescence spectra [28,29]. In this paper, we pursue our seminal investigation on a spiro[indoline-8-(benzothiazol-2-yl)-benzopyran] derivative (Scheme 1), whose metallochromic properties [30,31] and β contrasts [24,27] were previously reported, by analyzing its effectiveness to recognize alkali ions by means of variations in its linear and second-order nonlinear optical properties. In addition, we also concentrate on the thermodynamics of the cation complexation.

Scheme 1. Equilibrium between the spiropyran form and the merocyanine form complexing an alkali ion.

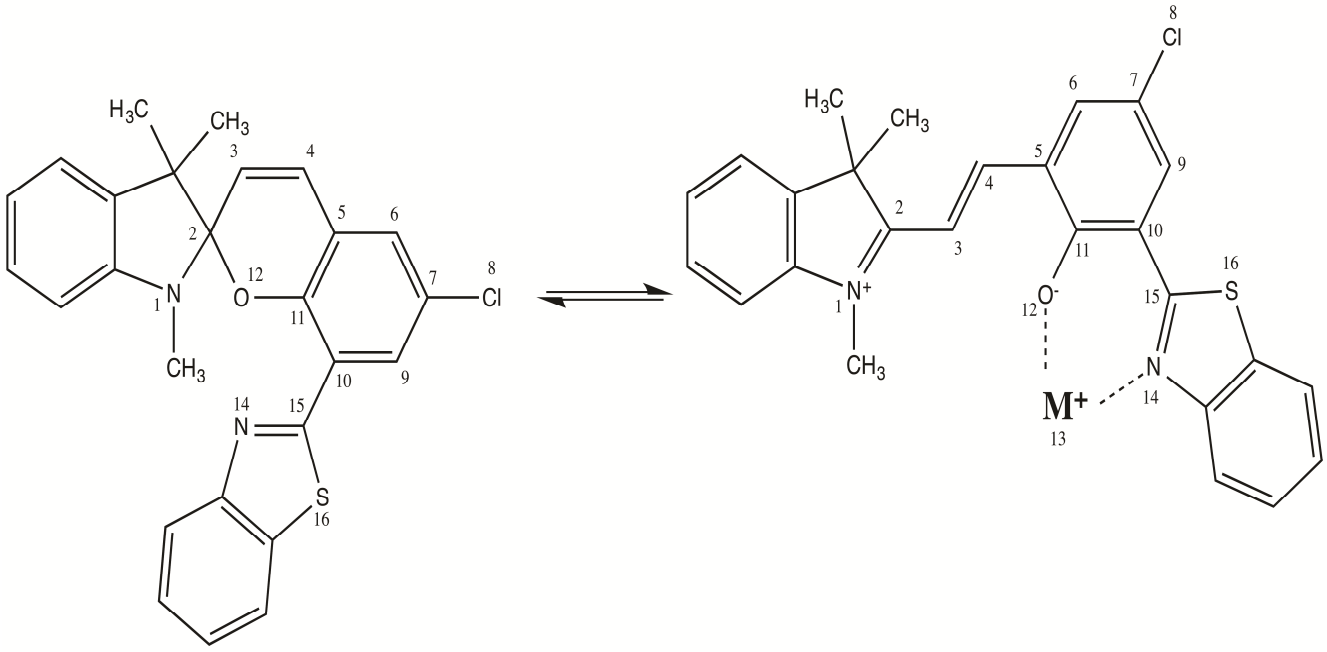

2. Results and Discussions

2.1. Molecular Structures and Thermodynamic Analysis

Representative bond lengths and torsion angles of the structures optimized in acetonitrile at the M06/6-311G*/Stuttgart1997 level are gathered in Table 1 for the spiropyran, the merocyanine, and the merocyanine complexing alkali ions. The largest variations appear for bonds 12–13 and 13–14 (ligand-metal, $d_{O\text{-}M}$ and $d_{N\text{-}M}$ distances) as well as 12–14 (claw opening distance), which evolves in parallel to the cation size, *i.e.*, $Li^+ < Na^+ < K^+ < Rb^+ < Cs^+$. Note that the $d_{O\text{-}M}$ distance is systematically shorter than the $d_{N\text{-}M}$ one, due to the generally larger negative charge on the oxygen ($q_O \in [-0.47, -0.54]$) compared to the nitrogen ($q_N \in [-0.41, -0.54]$), where q_O has been obtained from Mulliken population analysis. The reverse trend is observed for the 11–12 and 14–15 bond lengths, which get slightly smaller (and the bond stronger) when the cation is larger, evidencing a weaker complexation effect. The cation complexation has also an impact on the bond length alternation [BLA = ½ ($d_{2\text{-}3} + d_{4\text{-}5} - 2d_{3\text{-}4}$)] along the vinylic bridge linking the two aromatic moieties, which decreases from 0.039 Å for Li^+ to 0.021 Å for Cs^+. Indeed, a stronger complexation by the ligand induces the lengthening of the O-C bond, which then reduces the donor character of the ligand moiety (towards the accepting ring) and therefore increases the BLA. Owing to these π-conjugation effects and their modifications upon cation complexation, most bond lengths display systematic variations as a function of the cation size. Though the merocyanine moiety is planar, the $\theta_{11\text{-}12\text{-}13\text{-}14}$ dihedral angle increases significantly from Li^+ (13.1°) to Rb^+ (69.1°), which is related to the growing size of the cation and the need for a wider opening of the ligand claw.

Table 1. Bond lengths (Å), torsion angles (degrees), and bond length alternation [a] of the molecular structures optimized at the M06/6-311G*/Stuttgart1997 level. Solvent effects (CH_3CN) are included via the IEFPCM scheme. See Scheme 1 for the atom labels.

	Spiro	**Mero**	**Mero-Li^+**	**Mero-Na^+**	**Mero-K^+**	**Mero-Rb^+**	**Mero-Cs^+**
1-2	1.441	1.345	1.336	1.339	1.340	1.342	1.342
2-3	1.492	1.392	1.403	1.399	1.398	1.396	1.396
3-4	1.333	1.384	1.373	1.377	1.378	1.380	1.381
4-5	1.451	1.405	1.420	1.414	1.412	1.410	1.409
7-8	1.751	1.755	1.752	1.753	1.753	1.754	1.754
11-12	1.337	1.235	1.254	1.248	1.246	1.242	1.243
12-13	-	-	1.881	2.305	2.574	2.773	3.026
13-14	-	-	2.071	2.523	2.880	3.111	3.257
12-14	2.829	2.946	2.795	2.909	2.933	2.951	2.968
10-15	1.466	1.290	1.458	1.461	1.462	1.462	1.462
14-15	1.289	1.784	1.302	1.297	1.296	1.295	1.294
15-16	1.776	1.462	1.778	1.776	1.777	1.777	1.775
$\theta_{1\text{-}2\text{-}3\text{-}4}$	+135.7	+179.5	–179.7	–179.5	+179.2	–179.5	–179.2
$\theta_{2\text{-}3\text{-}4\text{-}5}$	+177.8	–179.7	–179.4	+178.2	–179.3	+179.9	+179.9
$\theta_{4\text{-}5\text{-}6\text{-}7}$	+177.9	–179.2	–179.5	+178.3	–178.9	+179.6	+179.8
$\theta_{11\text{-}12\text{-}13\text{-}14}$	-	-	+13.1	+44.5	+47.8	+52.7	+69.1
BLA	+0.139	+0.015	+0.039	+0.030	+0.027	+0.023	+0.022

[a] BLA = ½ ($d_{2\text{-}3} + d_{4\text{-}5} - 2\ d_{3\text{-}4}$).

The global charge of the different fragments (S_i) of the compounds were then computed at the M06/6-311G*/Stuttgart1997 level using the Mulliken approximation (Table 2). Upon complexing Cs^+ the modification of the charge distribution is mostly located on the nearby ligands, of which the electron density increases. Then, going towards smaller cations, this charge transfer effect is enhanced and the ligands get more negative while the cations get less and less positive. As a matter of fact, the resulting excess positive charge is distributed over the rest of the system, and particularly on the two closer aromatic rings (S_5 and S_9) but also, to a lower extent, on the merocyanine part. Switching between the spiropyran and merocyanine forms is also characterized by charge reorganizations, resulting from the opening of the spiro function.

Table 2. IEFPCM/M06/6-311G*/Stuttgart1997 Mulliken charge distribution for the fragments (S_1–S_{11}) of the spiropyran, merocyanine, and merocyanine-M^+.

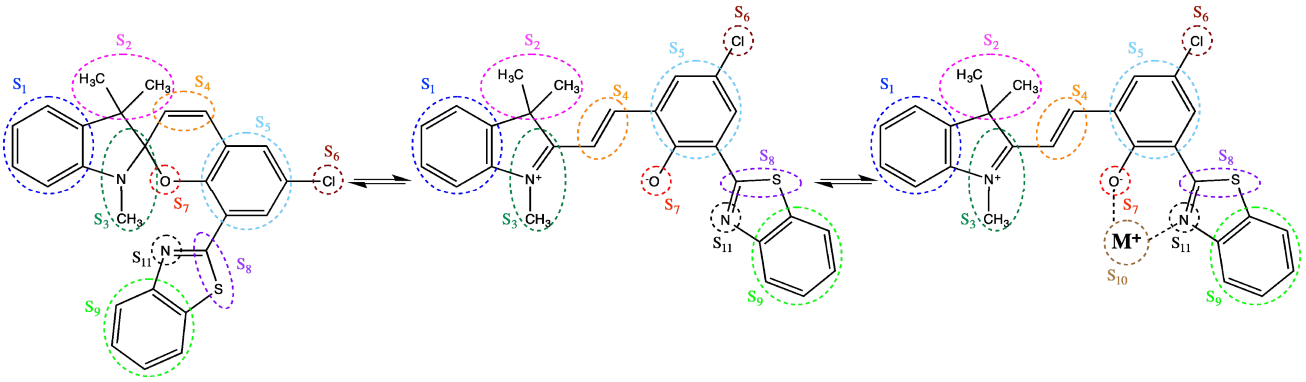

Fragments	Spiro	Mero	Mero-Li^+	Mero-Na^+	Mero-K^+	Mero-Rb^+	Mero-Cs^+
S_1	+0.240	+0.389	+0.426	+0.413	+0.410	+0.405	+0.404
S_2	+0.006	–0.025	–0.011	–0.016	–0.016	–0.018	–0.019
S_3	–0.100	+0.224	+0.257	+0.243	+0.243	+0.241	+0.240
S_4	+0.106	–0.115	–0.053	–0.075	–0.082	–0.099	–0.106
S_5	+0.259	+0.193	+0.296	+0.254	+0.241	+0.225	+0.197
S_6	–0.084	–0.105	–0.094	–0.098	–0.098	–0.100	–0.100
S_7	–0.382	–0.433	–0.538	–0.505	–0.500	–0.492	–0.470
S_8	+0.310	+0.263	+0.406	+0.343	+0.322	+0.302	+0.302
S_9	–0.009	–0.035	+0.072	+0.048	+0.029	+0.012	+0.011
S_{10}	-	-	+0.783	+0.866	+0.886	+0.942	+0.954
S_{11}	–0.346	–0.356	–0.544	–0.473	–0.435	–0.418	–0.413

Table 3 summarizes the main thermodynamic data for the complexation reaction of the alkali ion by the merocyanine form. The most exothermic reaction is the complexation of the largest cations (Rb^+ and Cs^+). The enthalpy of reaction evolves non-monotonically with the cation size, decreasing (in absolute value) from Li^+ to K^+, and then increasing to similar values for Rb^+ and Cs^+. To some extent, the Gibbs free energies behave similarly with the cation size, with however a more pronounced difference in the complexation energy of Li^+ compared to that of the largest cations. This is attributed to the larger amplitude of the entropy in the case of Li^+, due to the fact that the ligands are more tightly bound to the alkali atom. Indeed, the complexation reaction is accompanied by a decrease of the entropy and the

amplitude of that reduction tends to increase as a function of the covalent character of the cation-ligand bonds.

Table 3. Enthalpy, entropy, and Gibbs free enthalpy of reaction (kcal mol^{-1} except the entropies in cal mol^{-1} K^{-1}, at 298.15 K and 1 atm) for the complexation reaction calculated at the M06/6-311G* level in acetonitrile for different alkali cations.

Cations	ΔH^{θ}	ΔS^{θ}	ΔG^{θ}
Li^+	−15.5	−36.3	−4.8
Na^+	−11.0	−31.7	−1.6
K^+	−10.3	−26.4	−2.5
Rb^+	−17.3	−28.1	−9.0
Cs^+	−17.0	−25.9	−9.3

Selected vibrational frequencies calculated at the M06/6-311G* level in acetonitrile are listed in Table 4. Those around 1,600 wavenumber correspond to CO stretching vibrations and display a strong IR intensity. The frequency of these vibrational modes increases with the size of the cation. Indeed, smaller cations lead to a larger covalent character of the oxygen-metal bond, which translates into a smaller CO bond strength (as indicated by the increase of the CO bond length, see Table 1) and therefore into a smaller vibrational frequency. An opposite behavior is observed for the low frequency mode (684–495 cm^{-1}), which presents a strong O-cation and N-cation stretching character. In this case, the smaller the cation, the stronger the covalent bonds and the stronger the bond strengths.

Table 4. Frequencies (cm^{-1}) and IR intensities (km mol^{-1}) of selected vibrational modes for the merocyanine-M^+ systems calculated at the M06/6-311G* level in acetonitrile (IEF-PCM) for different alkali cations.

Cations	Frequency	IR Intensity
Li^+	695.2	1
	1574.8	309
	1626.0	660
Na^+	687.2	7
	1581.4	203
	1630.1	666
K^+	686.7	7
	1584.2	205
	1631.6	615
Rb^+	683.9	10
	1587.0	206
	1632.8	628
Cs^+	684.5	9
	1586.5	194
	1632.0	589

2.2. Linear Optical Properties

The values of the transition energies, wavelengths, and oscillator strengths calculated at the TDDFT/ωB97X level with the 6-311G*/Stuttgart1997 basis sets are gathered in Table 5. Owing to the formation of a π-conjugated segment between the donor and acceptor moieties, the breaking of the spiro junction results in a decrease of the first excitation energy by 1.6 eV and a substantial increase of the oscillator strength. Complexing the big Cs^+ atom leads to a small hypsochromic shift of the $S_0 \rightarrow S_1$ transition (7 nm or 0.03 eV) whereas going towards smaller cations, this shift increases up to 18 nm (0.11 eV), consistently with the increase of the BLA along the vinylic linker (Table 1). Note that this hypsochromic shift goes in the opposite direction to what was observed and calculated for coumarin 343 fluoroionophores [32]. The effect of the cation size on the oscillator strengths is negligible.

Table 5. Wavelengths (λ_{ge}, nm), transition energies (ΔE_{ge}, eV), oscillator strengths (f_{ge}) calculated at the TDDFT/ωB97X level with the 6-311G*/Stuttgart1997 basis sets for the different compounds. Solvent effects (CH_3CN) are included via the IEF-PCM scheme.

	λ_{ge} (nm)	ΔE_{ge}	f_{ge}
Spiro	294	4.21	0.260
Mero	474	2.62	1.071
Mero-Li^+	456	2.73	1.072
Mero-Na^+	461	2.69	1.074
Mero-K^+	463	2.68	1.066
Mero-Rb^+	466	2.66	1.059
Mero-Cs^+	467	2.65	1.059

2.3. Second-Order NLO Properties

Tables 6 and 7 report the static and dynamic HRS first hyperpolarizabilities (β_{HRS}), the depolarization ratios, as well as the β contrasts between the spiropyran and the merocyanine(-M^+) calculated in acetonitrile using different levels of approximation, namely HF, ωB97X, and MP2. The dynamic (λ = 1064 nm) MP2 values were estimated using Equation (1).

The (static and dynamic) β_{HRS} values increase upon including electron correlation at the MP2 level, are considered as reference. Compared to HF values, this increase is of 141, 36, 147, 110, 95, 83, and 63% respectively for the spiropyran, merocyanine and the merocyanine complexing Li^+, Na^+, K^+, Rb^+, and Cs^+. This results in variations of the first hyperpolarizability contrasts, in particular of the $\beta_{mero}/\beta_{spiro}$ contrast that decreases by about a factor of 2. When considering the ωB97X results, the electron correlation effects are about twice smaller than with the MP2 method. Except for the merocyanine where they lead to a decrease of β_{HRS} by 3%, the inclusion of electron correlation effects with the ωB97X functional enhances the HF β_{HRS} by 46%, 57%, 35%, 30%, 22%, and 16% for the spiropyran and the merocyanine complexing Li^+, Na^+, K^+, Rb^+, and Cs^+, respectively. These exaltation effects are much amplified when considering the dynamic β_{HRS} values, as a consequence of the smaller ωB97X excitation energies that lead to stronger frequency dispersion.

More importantly, the MP2 calculations evidence a strong enhancement of the β_{HRS} response of the merocyanine form upon complexation, whose amplitude increases inversely to the size of the alkali

ion. With the exception of Na^+ and K^+, which display similar NLO responses, the hyperpolarizabilities of the various merocyanine/cation complexes are significantly different, allowing unambiguous identification of the nature of the alkali metal. Similar trends are observed when using the ωB97X XC functional, whereas at the HF level the alkali complexation effects on β_{HRS} are much smaller and mainly go in the opposite direction. Besides, whatever the nature of the alkali, the complexation process does not induce remarkable variations in the values of the depolarization ratios (DR), which remain typical of one-dimensional π-conjugated systems dominated by a single diagonal β tensor component.

Table 6. Static (λ = ∞) and dynamic (λ = 1064 nm) HRS first hyperpolarizabilities, and depolarization ratios calculated at the HF, ωB97X, and MP2 levels with the 6-311+G*/Stuttgart1997 basis sets. Solvent effects (CH_3CN) are included via the IEF-PCM scheme.

λ (nm)	Property	Spiro	Mero	Mero-Li^+	Mero-Na^+	Mero-K^+	Mero-Rb^+	Mero-Cs^+
HF								
∞	β_{HRS}	196	3766	3369	3659	3755	3774	3744
	DR	4.16	3.18	3.38	3.40	3.39	3.31	3.31
1064	β_{HRS}	152	5568	5064	5523	5690	5654	5635
	DR	3.90	4.11	4.35	4.31	4.31	4.24	4.24
ωB97X								
∞	β_{HRS}	287	3660	5297	4950	4866	4593	4353
	DR	4.48	3.02	3.95	3.77	3.69	3.91	3.55
1064	β_{HRS}	240	11578	16234	15476	15294	14091	13847
	DR	5.22	4.64	4.89	4.87	4.86	4.81	4.80
MP2								
∞	β_{HRS}	473	5133	8290	7667	7617	6899	6095 [b]
	DR	4.56	3.17	4.55	4.01	4.15	3.92	3.74 [b]
1064	β_{HRS} [a]	367	7589	12461	11573	11542	10336	9173 [b]
	DR [a]	4.28	4.10	5.86	5.08	5.28	5.02	4.79 [b]

[a] Obtained with the multiplicative scheme, Equation (1); [b] Obtained with the 6-31G*/Stuttgart1997 basis sets.

Table 7. Static (λ = ∞) and dynamic (λ = 1064 nm) contrasts of HRS first hyperpolarizabilities of the spiropyran and the merocyanine(-M^+) at the HF, ωB97X, and MP2 levels with the 6-311+G*/Stuttgart1997 basis sets. Solvent effects (CH_3CN) are included via the IEF-PCM scheme.

Method	λ (nm)	$\frac{\beta_{mero}}{\beta_{spiro}}$	$\frac{\beta_{mero\text{-}Li^+}}{\beta_{spiro}}$	$\frac{\beta_{mero\text{-}Na^+}}{\beta_{spiro}}$	$\frac{\beta_{mero\text{-}K^+}}{\beta_{spiro}}$	$\frac{\beta_{mero\text{-}Rb^+}}{\beta_{spiro}}$	$\frac{\beta_{mero\text{-}Cs^+}}{\beta_{spiro}}$
HF	∞	19.2	17.2	18.7	19.2	19.3	19.1
	1064	36.6	33.3	36.3	37.4	37.2	37.1
ωB97X	∞	12.8	18.5	17.2	17.0	16.0	15.2
	1064	48.2	67.6	64.5	63.7	58.7	57.7
MP2	∞	10.9	17.5	16.2	16.1	14.6	16.6 [a]
	1064	20.7	34.0	31.5	31.4	28.2	32.2 [a]

[a] Obtained with the 6-31G*/Stuttgart1997 basis sets.

3. Computational Section

Geometry optimizations were performed at the density functional theory (DFT) level of approximation using the M06 exchange-correlation (XC) functional [33]. The 6-311G* basis set was used for all atoms except Rb and Cs, which were described by the Stuttgart 1997 basis set [34]. The components of the first hyperpolarizability tensor (β) were evaluated at different levels of approximation. The coupled-perturbed Hartree-Fock (CPHF) and the time-dependent Hartree-Fock (TDHF) approaches [35,36] were employed with the 6-311+G*/Stuttgart1997 basis sets to evaluate the static and dynamic (λ = 1064 nm) first hyperpolarizabilities, respectively. Secondly, in order to account for electron correlation effects, the static β components were computed by employing the second-order Møller-Plesset level (MP2) in combination with the finite field (FF) procedure [37] using the same basis sets. In these FF calculations, the higher-order contaminations were removed by adopting the usual Romberg procedure [38–40]. Then, the HF and MP2 results were combined in order to predict approximate dynamic MP2 values. This was achieved by using the multiplicative scheme [41–43], which consists in multiplying the static MP2 value by a corrective dispersion factor:

$$\beta_{MP2}(-2\omega;\omega,\omega) \simeq \beta_{MP2}(0;0,0)\frac{\beta_{TDHF}(-2\omega;\omega,\omega)}{\beta_{CPHF}(0;0,0)} \quad (1)$$

Additional calculations of the first hyperpolarizability were performed at the time-dependent density functional theory (TDDFT) level with the ωB97X XC functional [44]. This functional includes 15.77% and 84.23% of exact HF exchange at short- and long-range, respectively, and is among the best XC functionals to predict the excitation energies of push-pull π-conjugated systems. Among second-order NLO phenomena, we focused on the hyper-Rayleigh scattering (HRS) response, $\beta_{HRS}(-2\omega;\omega,\omega) = \beta_{HRS}$ [45]. Assuming a non-polarized incident light propagating along the Y direction (in the laboratory frame), the intensity of the harmonic light scattered at 90° along the X direction and vertically (V) polarized (along the Z axis) is given by Bersohn's expression [46]:

$$\beta_{HRS} = \sqrt{\left\{\left\langle \beta_{ZZZ}^2 \right\rangle + \left\langle \beta_{ZXX}^2 \right\rangle\right\}} \quad (2)$$

The depolarization ratio, DR, which reveals the shape of the NLO-phore, reads:

$$DR = \frac{I_{VV}^{2\omega}}{I_{HV}^{2\omega}} = \frac{\left\langle \beta_{ZZZ}^2 \right\rangle}{\left\langle \beta_{ZXX}^2 \right\rangle} \quad (3)$$

where $\left\langle \beta_{ZZZ}^2 \right\rangle$ and $\left\langle \beta_{ZXX}^2 \right\rangle$ are orientational averages of β tensor components, which are proportional to the scattered signal intensities for vertically and horizontally-polarized incident signals, respectively. The orientational averages in Equations (2) and (3) were calculated without assuming Kleinman's conditions, *i.e.*, without applying permutation symmetry rules on the Cartesian components of the hyperpolarizability tensor. All reported β values are given in atomic units [1 a.u. of β = 3.62×10^{-42} m^4 V^{-1} = 3.2063×10^{-53} C^3 m^3 J^{-2} = 8.641×10^{-33} esu] within the T convention of [47].

The vertical excitation energies (ΔE_{ge}) and the corresponding wavelength λ_{ge} were calculated at the TDDFT level using the range-separated hybrid functional ωB97X and the combination of the 6-311G(d)/Stuttgart1997 basis sets.

Solvent effects on the linear and nonlinear optical properties were accounted by using the polarizable continuum model within the integral equation formalism (IEF-PCM) [48,49]. This model describes the molecular environment as a structureless polarizable continuum characterized by its macroscopic dielectric permittivity, ε_ω, which depends on the frequency ω of the applied electric field. All the calculations were performed in acetonitrile (CH_3CN: $\varepsilon_0 = 36.64$, $\varepsilon_\infty = 1.806$), using the Gaussian 09 package [50].

4. Conclusions

Structural, thermodynamical, vibrational, as well as linear and nonlinear optical properties of a spiro[indoline-8-(benzothiazol-2-yl)-benzopyran] derivative and of its merocyanine form have been evaluated by using first principles methods. In particular, calculations are used to unravel the variations of these properties that occur when the merocyanine form complexes alkali cations of increasing size, from Li^+ to Cs^+. The following trends have been observed, (i) the complexation of smaller cations leads to the formation of stronger metal-ligand bonds, larger geometrical relaxations, and larger charge redistributions over the whole system, that result in a stronger hypsochromic shift of the first excitation energy and in a larger enhancement of the first hyperpolarizability, (ii) these structural, electronic, vibrational, and optical properties are less impacted by the complexation of larger cations, and (iii) the enthalpies of complexation show a minimum for the Na^+ and K^+ cations for which the covalent bond is weaker than in the case of Li^+, whereas the opening of the claw is too large to match the cation size as in the case of Rb^+ and Cs^+. The broad range of variation of the first hyperpolarizability as a function of the cation size confirms the potential of the second-order NLO responses of this merocyanine for detecting and identifying metal cation.

Acknowledgments

A.P. thanks the F.R.S.-FNRS for her postdoctoral researcher position. This work has been supported by funds from the CNRS, the Région Aquitaine, the F.R.S.-FNRS, the AUL (ARC TinTin), and by the Belgian Government (IUAP No. P7/5). The calculations were performed on the computing facilities of the Consortium des Équipements de Calcul Intensif (CÉCI, http://www.ceci-hpc.be), in particular those of the Plateforme Technologique de Calcul Intensif (PTCI) installed in the University of Namur, for which we gratefully acknowledge financial support of the FNRS-FRFC (Convention No. 2.4.617.07.F and 2.5020.11) and of the University of Namur.

Author Contributions

A.P. performed the calculations; A.P., B.C., and F.C. analyzed the data and wrote the manuscript.

Conflicts of Interest

The authors declare no conflict of interest.

References

1. Coe, B.J. Molecular Materials possessing switchable quadratic nonlinear optical properties. *Chem. Eur. J.* **1999**, *5*, 2464–2471.
2. Delaire, J.A.; Nakatani, K. Linear and nonlinear optical properties of photochromic molecules and materials. *Chem. Rev.* **2000**, *100*, 1817–1845.
3. Asselberghs, I.; Clays, K.; Persoons, A.; Ward, M.D.; McCleverty, J. Switching of molecular second-order polarisability in solution. *J. Mater. Chem*. **2004**, *14*, 2831–2839.
4. Castet, F.; Rodriguez, V.; Pozzo, J.L.; Ducasse, L.; Plaquet, A.; Champagne, B. Design and characterization of molecular nonlinear optical switches. *Acc. Chem Res.* **2013**, *46*, 2656–2665.
5. Christodoulides, D.N.; Khoo, I.C.; Salamo, G.J.; Stegeman, G.I.; Van Stryland, E.W. Nonlinear refraction and absorption mechanisms and magnitudes, *Adv. Opt. Photonics* **2010**, *2*, 60–200.
6. Stegeman, G.I.; Stegeman, R.A. *Nonlinear Optics: Phenomena, Materials, and Devices*; Wiley Series in Pure and Applied Optics; Boreman, G., Series Ed.; John Wiley & Sons: Hoboken, NJ, USA, 2012.
7. Sanguinet, L.; Pozzo, J.L.; Rodriguez, V.; Adamietz, F.; Castet, F.; Ducasse, L.; Champagne, B. Acido- and Phototriggered NLO properties enhancement. *J. Phys. Chem. B* **2005**, *109*, 11139–11150.
8. Plaquet, A.; Champagne, B.; Kulhánek, J.; Bureš, F.; Bogdan, E.; Castet, F.; Ducasse, L.; Rodriguez, V. Effects of the nature and length of the π-conjugated bridge on the second-order nonlinear optical responses of push-pull molecules including 4, 5-Dicyanoimidazole and their protonated forms. *Chem. Phys. Chem.* **2011**, *11*, 3245–3252.
9. Cariati, E.; Dragonetti, C.; Lucenti, E.; Nisic, F.; Righetto, S.; Roberto, D.; Tordin, E. An acido-triggered reversible luminescent and nonlinear optical switch based on a substituted styrylpyridine: EFISH measurements as an unusual method to reveal a protonation-deprotonation NLO contrast. *Chem. Commun.* **2014**, *50*, 1608–1610.
10. Sliwa, M.; Spangenberg, A.; Malfant, I.; Lacroix, P.G.; Métivier, R.; Pansu, R.B.; Nakatani, K. Structural, optical, and theoretical studies of a thermochromic organic crystal with reversibly variable second harmonic generation. *Chem. Mater.* **2008**, *20*, 4062–4068.
11. Sliwa, M.; Létard, S.; Malfant, I.; Nierlich, M.; Lacroix, P.G.; Asahi, T.; Masuhara, H.; Yu, P.; Nakatani, K. Design, synthesis, structural, and nonlinear optical properties of photochromic crystals: Toward reversible molecular switches. *Chem. Mater.* **2005**, *17*, 4727–4735.
12. Aubert, V.; Guerchais, V.; Ishow, E.; Hoang-Thi, K.; Ledoux, I.; Nakatani, K.; le Bozec, H. Efficient photoswitching of the nonlinear optical properties of dipolar photochromic zinc(II) complexes. *Angew. Chem. Int. Ed.* **2008**, *47*, 577–580.
13. Nitadori, H.; Ordronneau, L.; Boixel, J.; Jacquemin, D.; Boucekkine, A.; Singh, A.; Akita, M.; Ledoux, I.; Guerchais, V.; le Bozec, H. Photoswitching of the second-order nonlinearity of a tetrahedral octupolar multi DTE-based copper(I) complex. *Chem. Commun.* **2012**, *48*, 10395–10397.
14. Coe, B.J.; Houbrechts, S.; Asselberghs, I.; Persoons, A. Efficient, reversible redox-switching of molecular first hyperpolarizabilities in ruthenium(II) complexes possessing large quadratic optical nonlinearities. *Angew. Chem. Int. Ed.* **1999**, *38*, 366–369.

15. Boubekeur-Lecaque, L.; Coe, B.J.; Clays, K.; Foerier, S.; Verbiest, T.; Asselberghs, I. Redox-switching of nonlinear optical behavior in langmuir-blodgett thin films containing a ruthenium(II) ammine complex. *J. Am. Chem. Soc.* **2008**, *130*, 3286–3287.
16. Liu, C.G.; Guan, X.H.; Su, Z.M. Computational study on redox-switchable 2D second-order nonlinear optical properties of push–pull mono-tetrathiafulvalene-bis(Salicylaldiminato) Zn(II) schiff base complexes. *J. Phys. Chem. C* **2011**, *115*, 6024–6032.
17. Gauthier, N.; Argouarch, G.; Paul, F.; Toupet, L.; Ladjarafi, A.; Costuas, K.; Halet, J.F.; Samoc, M.; Cifuentes, M.P.; Corkery, T.C.; *et al.* Electron-rich iron/ruthenium arylalkynyl complexes for third-order nonlinear optics: redox-switching between three states. *Chem. Eur. J.* **2011**, *17*, 5561–5577.
18. Mançois, F.; Sanguinet, L.; Pozzo, J.L.; Guillaume, M.; Champagne, B.; Rodriguez, V.; Adamietz, F.; Ducasse, L.; Castet, F. Acido-triggered nonlinear optical switches: Benzazolo-oxazolidines. *J. Phys. Chem. B* **2007**, *111*, 9795–9802.
19. Mançois, F.; Pozzo, J.L.; Pan, J.; Adamietz, F.; Rodriguez, V.; Ducasse, L.; Castet, F.; Plaquet, A.; Champagne, B. Two-way molecular switches with large nonlinear optical contrast. *Chem. Eur. J.* **2009**, *15*, 2560–2571.
20. Sliwa, M.; Nakatani, K.; Asahi, T.; Lacroix, P.G.; Pansu, R.B.; Masuhara, H. Polarization and wavelength dependent nonlinear optical properties of a photo-switchable organic crystal. *Chem. Phys. Lett.* **2007**, *437*, 212–217.
21. Plaquet, A.; Guillaume, M.; Champagne, B.; Rougier, L.; Mançois, F.; Rodriguez, V.; Pozzo, J.L.; Ducasse, L.; Castet, F. Investigation on the second-order nonlinear optical responses in the keto-enol equilibrium of anil derivatives. *J. Phys. Chem. C* **2008***, 12*, 5638–5645.
22. Bogdan, E.; Plaquet, A.; Antonov, L.; Rodriguez, V.; Ducasse, L.; Champagne, B.; Castet, F. Solvent effects on the second-order nonlinear optical responses in the keto-enol equilibrium of a 2-hydroxy-1-naphthaldehyde derivative. *J. Phys. Chem. C* **2010**, *114*, 12760–12768.
23. Ségerie, A.; Castet, F.; Kanoun, M.B.; Plaquet, A.; Liégeois, V.; Champagne, B. Nonlinear optical switching behavior in the solid state: A theoretical investigation on anils. *Chem. Mater.* **2011**, *23*, 3993–4001.
24. Plaquet, A.; Guillaume, M.; Champagne, B.; Castet, F.; Ducasse, L.; Pozzo, J.L.; Rodriguez, V. *In silico* optimization of merocyanine-spiropyran compounds as second-order nonlinear optical molecular switches. *Phys. Chem. Chem. Phys.* **2008**, *10*, 6223–6232.
25. Valeur, B.; Leray, I. Design principles of fluorescent molecular sensors for cation recognition. *Coord. Chem. Rev.* **2000**, *205*, 3–40.
26. De Silva, A.P.; Vance, T.P.; West, M.E.S.; Wright, G.D. Bright molecules with sense, logic, numeracy and utility. *Org. Biomol. Chem.* **2008**, *6*, 2468–2480.
27. Champagne, B.; Plaquet, A.; Pozzo, J.L.; Rodriguez, V.; Castet, F. Nonlinear optical molecular switches as selective cation sensors. *J. Am. Chem. Soc.* **2012**, *134*, 8101–8103.
28. Zakharova, M.I.; Coudret, C.; Pimienta, V.; Micheau, J.C.; Delbaere, S.; Vermeersch, G.; Metelitsa, A.V.; Voloshin, N.; Minkin, V.I. Quantitative investigations of cation complexation of photochromic 8-benzothiazole-substituted benzopyran: Towards metal-ion sensors. *Photochem. Photobiol. Sci.* **2010**, *9*, 199–207.

29. Valeur, B. Molecular Fluorescence: Principles and Applications; Wiley-VCH: Berlin, Germany, 2001.
30. Alhashimy, N.; Byrne, R.; Minkovska, S.; Diamond, D. Novel synthesis and characterisation of 3,3-dimethyl-5'-(2-benzothiazolyl)-spironaphth(indoline-2,3'-[3*H*]naphth[2,1-*b*][1,4]oxazine) derivatives. *Tetrahedron Lett.* **2009**, *50*, 2573–2576.
31. Paramonov, S.V.; Lokshin, V.; Fedorova, O.A. Spiropyran, chromene or spirooxazine ligands: insights into mutual relations between complexing and photochromic properties. *J. Photochm. Photobiol. C* **2011**, *12*, 209–236.
32. Botek, E.; d'Antuono, P.; Jacques, A.; Carion, R.; Champagne, B.; Maton, L.; Taziaux, D.; Habib-Jiwan, J.L. Theoretical and experimental investigation of the structural and spectroscopic properties of coumarin 343 fluoroionophores. *Phys. Chem. Chem. Phys.* **2010**, *12*, 14172–14187.
33. Zhao, Y.; Truhlar, D.G. The M06 suite of density functionals for main group thermochemistry, thermochemical kinetics, noncovalent interactions, excited states, and transition elements: Two new functionals and systematic testing of four M06-class functionals and 12 other functionals. *Theor. Chem. Acc.* **2008**, *120*, 215–241.
34. Kaupp, M.; Schleyer, P.V.R.; Stoll, H.; Preuss, H. Pseudopotential approaches to Ca, Sr, and Ba hydrides. Why are some alkaline earth MX_2 compounds bent? *J. Chem. Phys.* **1991**, *94*, 1360–1366.
35. Sekino, H.; Bartlett, R.J. Frequency dependent nonlinear optical properties of molecules. *J. Chem. Phys.* **1986**, *85*, 976–989.
36. Karna, S.P.; Dupuis, M. Frequency dependent nonlinear optical properties of molecules: Formulation and implementation in the HONDO program. *J. Comp. Chem.* **1991**, *12*, 487–504.
37. Cohen, H.D.; Roothaan, C.C.J. Electric dipole polarizability of atoms by the Hartree-Fock method. I. Theory for closed-shell systems. *J. Chem. Phys*. **1965**, *43*, S34–S39.
38. Davis, P.J.; Rabinowitz, P. *Numerical Integration*; Blaisdell Publishing Company: London, UK, 1967.
39. Mohammed, A.A.K.; Limacher, P.A.; Champagne, B. Finding optimal finite field strengths allowing for a maximum of precision in the calculation of polarizabilities and hyperpolarizabilities. *J. Comput. Chem.* **2013**, *34*, 1497–1507.
40. De Wergifosse, M.; Liégeois, V.; Champagne, B. Evaluation of the molecular static and dynamic first hyperpolarizabilities. *Int. J. Quantum. Chem.* **2014**, *114*, 900–910.
41. Sekino, H.; Bartlett, R.J. Hyperpolarizabilities of the hydrogen fluoride molecule: A discrepancy between theory and experiment? *J. Chem. Phys.* **1986**, *84*, 2726–2733.
42. Rice, J.E.; Handy, N.C. The calculation of frequency-dependent hyperpolarizabilities including electron correlation effects. *Int. J. Quantum Chem.* **1992**, *43*, 91–118.
43. Jacquemin, D.; Champagne, B.; Hättig, C. Correlated frequency-dependent electronic first hyperpolarizability of small push–pull conjugated chains. *Chem. Phys. Lett.* **2000**, *319*, 327–334.
44. Chai, J.D.; Head-Gordon, M. Systematic optimization of long-range corrected hybrid density functionals. *J. Chem. Phys.* **2008**, *128*, doi:http://dx.doi.org/10.1063/1.2834918.
45. Verbiest, T.; Clays, K.; Rodriguez, V. *Second-Order Nonlinear Optical Characterizations Techniques: An Introduction*; CRC Press: New York, NY, USA, 2009.
46. Bersohn, R.; Pao, Y.H.; Frisch, H.L. Double-quantum light scattering by molecules. *J. Chem. Phys.* **1966**, *45*, 3184–3198.

47. Willetts, A.; Rice, J.E.; Burland, D.A.; Shelton, D.P. Problems in the comparison of theoretical and experimental hyperpolarizabilities. *J. Chem. Phys.* **1992**, *97*, 7590–7599.
48. Tomasi, J.; Persico, M. Molecular interactions in solution: An overview of methods based on continuous distributions of the solvent. *Chem. Rev.* **1994**, *94*, 2027–2094.
49. Tomasi, J.; Mennucci, B.; Cammi, R. quantum mechanical continuum solvation models. *Chem. Rev.* **2005**, *105*, 2999–3094.
50. Frisch, M.J.; Trucks, G.W.; Schlegel, H.B.; Scuseria, G.E.; Robb, M.A.; Cheeseman, J.R.; Scalmani, G.; Barone, V.; Mennucci, B.; Petersson, G.A.; *et al. Gaussian 09*, Revision A.02; Gaussian, Inc.: Wallingford, CT, USA, 2009.

Sample Availability: Not available.